Supplementary Material for:
Nonequilibrium steady-state picture of photosynthetic light harvesting

Veljko Janković[1, a)] and Tomáš Mančal[2, b)]
[1)] *Scientific Computing Laboratory, Center for the Study of Complex Systems, Institute of Physics Belgrade, University of Belgrade, Pregrevica 118, 11080 Belgrade, Serbia*
[2)] *Faculty of Mathematics and Physics, Charles University, Ke Karlovu 5, 121 16 Prague 2, Czech Republic*

SI. DERIVATION OF EXPRESSIONS FOR TRANSFORMATION PARAMETERS θ AND Δ

Here, we discuss in greater detail the expressions for the transformation parameters θ_{px} and Δ_{px} between the exciton basis and the preferred basis of the NESS. The discussion in the case of localized basis is analogous.

The normalized RDM in the ee sector, $\widetilde{\rho}^{ss}_{ee}$, is expressed in the preferred basis of the NESS and the exciton basis as follows

$$\widetilde{\rho}^{ss}_{ee} = \sum_i \widetilde{p}_i \, |p_i\rangle\langle p_i| = \sum_{jk} \left(\sum_i \langle x_j|p_i\rangle \widetilde{p}_i \langle p_i|x_k\rangle \right) |x_j\rangle\langle x_k|. \tag{S1}$$

On the other hand, the expression for $\widetilde{\rho}^{ss}_{ee}$ in terms of Pauli matrices

$$\sigma_1 = |x_0\rangle\langle x_1| + |x_1\rangle\langle x_0|, \quad \sigma_2 = -\mathrm{i}\left(|x_0\rangle\langle x_1| - |x_1\rangle\langle x_0|\right), \quad \sigma_3 = |x_0\rangle\langle x_0| - |x_1\rangle\langle x_1| \tag{S2}$$

reads as

$$\widetilde{\rho}^{ss}_{ee} = \frac{1}{2}\left((1+a^x_3)|x_0\rangle\langle x_0| + (a^x_1 - \mathrm{i}a^x_2)|x_0\rangle\langle x_1| + (a^x_1 + \mathrm{i}a^x_2)|x_1\rangle\langle x_0| + (1-a^x_3)|x_1\rangle\langle x_1|\right). \tag{S3}$$

Using Eqs. (S1) and (S3) together with Eq. (23) of the main text we obtain

$$a^x_3 = (2\widetilde{p}_0 - 1)\cos(2\theta_{px}) = (1 - 2\widetilde{p}_1)\cos(2\theta_{px}) \tag{S4}$$

$$a^x_1 - \mathrm{i}a^x_2 = (2\widetilde{p}_0 - 1)\,\mathrm{e}^{\mathrm{i}2\Delta_{px}}\sin(2\theta_{px}). \tag{S5}$$

The relationships between the Bloch angles θ^x_B and ϕ^x_B and transformation parameters θ_{px} and Δ_{px} that presented in the main body of the manuscript now become apparent.

Let us now discuss the range in which θ_{px} and Δ_{px} may always be chosen. The Pauli matrices may be chosen as in Eq. (S2) and we this choice will be termed choice 1. There is, however, choice 2, in which $|x_0\rangle$ and $|x_1\rangle$ are permuted

$$\sigma_1 = |x_1\rangle\langle x_0| + |x_0\rangle\langle x_1|, \quad \sigma_2 = -\mathrm{i}\left(|x_1\rangle\langle x_0| - |x_0\rangle\langle x_1|\right), \quad \sigma_3 = |x_1\rangle\langle x_1| - |x_0\rangle\langle x_0|. \tag{S6}$$

Then, $a^{x,(1)}_3 = -a^{x,(2)}_3$, $a^{x,(1)}_2 = -a^{x,(2)}_2$, and $a^{x,(1)}_1 = a^{x,(2)}_1$, so that

$$\cos(2\theta^{(1)}_{px}) + \cos(2\theta^{(2)}_{px}) = 2\cos(\theta^{(1)}_{px} + \theta^{(2)}_{px})\cos(\theta^{(1)}_{px} - \theta^{(2)}_{px}) = 0, \tag{S7}$$

$$\tan(2\Delta^{(1)}_{px}) + \tan(2\Delta^{(2)}_{px}) = \left(1 - \tan(2\Delta^{(1)}_{px})\tan(2\Delta^{(2)}_{px})\right)\tan(2\Delta^{(1)}_{px} + 2\Delta^{(2)}_{px}) = 0. \tag{S8}$$

It then follows that (k is an integer)

$$\theta^{(2)}_{px} = \frac{\pi}{2} \pm \theta^{(1)}_{px} + k\pi, \quad \Delta^{(2)}_{px} = -\Delta^{(1)}_{px} + k\frac{\pi}{2}. \tag{S9}$$

From Eq. (S4), we know that $\theta^{(1)}_{px} \in (0, \pi/2)$, so that the rotation angle $\theta^{(2)}_{px}$ can always be chosen so than $\theta^{(2)}_{px} \in (0, \pi/4)$. Equation (S9) suggests that such a choice for θ_{px} may result in the phase Δ_{px} acquiring an additional minus sign, which, however, does not affect the range $(-\pi/4, \pi/4)$ of possible values for Δ_{px}. It is for this reason that in Figs. 2–7 of the main text we plot the magnitude $|\Delta_{px}|$.

[a)] Electronic mail: veljko.jankovic@ipb.ac.rs
[b)] Electronic mail: mancal@karlov.mff.cuni.cz

SII. COMPUTATION OF THE NONEQUILIBRIUM STEADY STATE

As mentioned in the main body of the manuscript, the computational algorithm to obtain the NESS leans on the method proposed in Ref. 1 to compute the excited-state equilibrium of a molecular aggregate. The method exploits the fact that the computation of the HEOM steady state can be seen as solving a system of linear algebraic equations, which can be done in an iterative way using, e.g., the Jacobi iteration method. However, the Jacobi iteration method relies on the diagonal dominance of the system, an assumption that is, in general, not satisfied in our problem, especially in the regimes of intermediate and strong system–bath coupling. Equations (10) and (11) of the main text are the basis for the following iterative procedure to compute the ADMs $\sigma^{ss,\mathrm{new}}_{eg,\mathbf{n}}$ and $\sigma^{ss,\mathrm{new}}_{ee,\mathbf{n}}$ in the current iteration using the ADMs $\sigma^{ss,\mathrm{old}}_{eg,\mathbf{n}}$ and $\sigma^{ss,\mathrm{old}}_{ee,\mathbf{n}}$ from the previous iteration

$$
\begin{aligned}
\left(\mathrm{i}\frac{\omega_x-\omega_c}{\gamma}+\frac{\gamma_{\mathbf{n}}}{\gamma}+(\tau_c\gamma)^{-1}+\epsilon\right)\left\langle x\left|\sigma^{ss,\mathrm{new}}_{eg,\mathbf{n}}\right|g\right\rangle &= \epsilon\left\langle x\left|\sigma^{ss,\mathrm{old}}_{eg,\mathbf{n}}\right|g\right\rangle-\frac{\Delta}{\hbar^2\gamma}\sum_j\left\langle x\left|V_j\sigma^{ss,\mathrm{old}}_{eg,\mathbf{n}}\right|g\right\rangle\\
&+\delta_{\mathbf{n},\mathbf{0}}\frac{\mathrm{i}}{\hbar\gamma}I_0\langle x|\mu_{eg}|g\rangle\\
&+\mathrm{i}\sum_j\sum_{m=0}^{K-1}\sqrt{1+n_{j,m}}\sqrt{\frac{|c_m|}{(\hbar\gamma)^2}}\left\langle x\left|V_j\sigma^{ss,\mathrm{old}}_{eg,\mathbf{n}^+_{j,m}}\right|g\right\rangle\\
&+\mathrm{i}\sum_j\sum_{m=0}^{K-1}\sqrt{n_{j,m}}\frac{c_m/(\hbar\gamma)^2}{\sqrt{|c_m|/(\hbar\gamma)^2}}\left\langle x\left|V_j\sigma^{ss,\mathrm{old}}_{eg,\mathbf{n}^-_{j,m}}\right|g\right\rangle
\end{aligned}
\tag{S10}
$$

$$
\begin{aligned}
\left(\mathrm{i}\frac{\omega_x-\omega_{\bar{x}}}{\gamma}+\frac{\gamma_{\mathbf{n}}}{\gamma}+\epsilon\right)\left\langle x\left|\sigma^{ss,\mathrm{new}}_{ee,\mathbf{n}}\right|\bar{x}\right\rangle &= \epsilon\left\langle x\left|\sigma^{ss,\mathrm{old}}_{ee,\mathbf{n}}\right|\bar{x}\right\rangle-\frac{\Delta}{\hbar^2\gamma}\sum_j\left\langle x\left|V_j^{\times}V_j^{\times}\sigma^{ss,\mathrm{old}}_{ee,\mathbf{n}}\right|\bar{x}\right\rangle\\
&+\frac{\mathrm{i}}{\hbar\gamma}\langle x|\mu_{eg}|g\rangle\left\langle\bar{x}\left|\sigma^{ss,\mathrm{old}}_{eg,\mathbf{n}}\right|g\right\rangle^*-\frac{\mathrm{i}}{\hbar\gamma}\left\langle x\left|\sigma^{ss,\mathrm{old}}_{eg,\mathbf{n}}\right|g\right\rangle\langle\bar{x}|\mu_{eg}|g\rangle^*\\
&+\gamma^{-1}\left\langle x\left|\mathcal{L}_{\mathrm{rec}}[\sigma^{ss,\mathrm{old}}_{ee,\mathbf{n}}]\right|\bar{x}\right\rangle+\gamma^{-1}\left\langle x\left|\mathcal{L}_{\mathrm{RC}}[\sigma^{ss,\mathrm{old}}_{ee,\mathbf{n}}]\right|\bar{x}\right\rangle\\
&+\mathrm{i}\sum_j\sum_{m=0}^{K-1}\sqrt{1+n_{j,m}}\sqrt{\frac{|c_m|}{(\hbar\gamma)^2}}\left\langle x\left|V_j^{\times}\sigma^{ss,\mathrm{old}}_{ee,\mathbf{n}^+_{j,m}}\right|\bar{x}\right\rangle\\
&+\mathrm{i}\sum_j\sum_{m=0}^{K-1}\sqrt{n_{j,m}}\frac{c_m/(\hbar\gamma)^2}{\sqrt{|c_m|/(\hbar\gamma)^2}}\left\langle x\left|V_j\sigma^{ss,\mathrm{old}}_{ee,\mathbf{n}^-_{j,m}}\right|\bar{x}\right\rangle\\
&-\mathrm{i}\sum_j\sum_{m=0}^{K-1}\sqrt{n_{j,m}}\frac{c_m^*/(\hbar\gamma)^2}{\sqrt{|c_m|/(\hbar\gamma)^2}}\left\langle x\left|\sigma^{ss,\mathrm{old}}_{ee,\mathbf{n}^-_{j,m}}V_j\right|\bar{x}\right\rangle
\end{aligned}
\tag{S11}
$$

In Eqs. (S10) and (S11), $|x\rangle$ and $|\bar{x}\rangle$ are exciton states, $\hbar\omega_x$ and $\hbar\omega_{\bar{x}}$ are their respective vertical excitation energies, while ϵ is an adjustable parameter whose value should be tuned so that the steady-state HEOM becomes a diagonally dominant system of linear algebraic equations. The value of ϵ should be chosen so as to reach a compromise between algorithm stability and numerical accuracy (large ϵ) on the one hand and numerical effort (small ϵ) on the other hand.

Equations (S10) and (S11) are solved in the exciton basis because their free-evolution parts are diagonal in that basis, see the c-numbers that multiply the ADM elements in the current iteration on the left-hand sides of these equations. When the trapping and/or recombination Liouvillians are known to be diagonal in the exciton basis, they may be treated in the same manner as the free-evolution terms, which would lead to a more complicated form of the c-numbers appearing on the left-hand sides of Eqs. (S10) and (S11).

The iterative procedure is terminated once the continuity equation [Eq.(...) of the main text] is satisfied with the desired numerical accuracy δ. In more detail, we use the following termination criterion

$$
\frac{|J_{\mathrm{gen}}-J_{\mathrm{RC}}-J_{\mathrm{rec}}|}{\min\{J_{\mathrm{gen}},J_{\mathrm{RC}},J_{\mathrm{rec}}\}}<\delta. \tag{S12}
$$

Our numerical computations suggest that the quantity on the left-hand side of Eq. (S12) monotonously decreases as the algorithm proceeds, so that the termination criterion is sensible. We also monitor changes the ADM elements

undergo upon one iteration of the algorithm by following the changes in the following quantities

$$E_{ee} = \max_{\mathbf{n},\bar{x},x} \left\{ [f(\mathbf{n})]^{-1} \left| \left\langle x \left| \sigma_{ee,\mathbf{n}}^{ss,\mathrm{new}} \right| \bar{x} \right\rangle - \left\langle x \left| \sigma_{ee,\mathbf{n}}^{ss,\mathrm{old}} \right| \bar{x} \right\rangle \right| \right\}, \tag{S13}$$

$$E_{eg} = \max_{\mathbf{n},\bar{x},x} \left\{ [f(\mathbf{n})]^{-1} \left| \left\langle x \left| \sigma_{eg,\mathbf{n}}^{ss,\mathrm{new}} \right| \bar{x} \right\rangle - \left\langle x \left| \sigma_{eg,\mathbf{n}}^{ss,\mathrm{old}} \right| \bar{x} \right\rangle \right| \right\}, \tag{S14}$$

where the rescaling factor $f(\mathbf{n})$ reads as[2]

$$f(\mathbf{n}) = \prod_{j} \prod_{m=0}^{K-1} \left[\left(\frac{|c_m|}{(\hbar\gamma)^2} \right)^{n_{j,m}} n_{j,m}! \right]^{-1/2}. \tag{S15}$$

We observe that the quantities E_{ee} and E_{eg} monotonically decrease during the course of the algorithm, another sign that our procedure for determining the NESS should lead to correct results.

Another important ingredient of the algorithm is the initial guess for the iterative procedure embodied in Eqs. (S10) and (S11). In Ref. 1, which dealt with the excited-state equilibrium, the initial condition was the purely electronic density matrix in the absence of the environment, i.e., $e^{-\beta H_M}/\mathrm{Tr}_M\left\{e^{-\beta H_M}\right\}$. Here, however, we have incoherent driving, trapping, and recombination, so that a natural initial guess for the NESS can be obtained by solving the corresponding Redfield equation. In our companion paper, we presented the derivation of the Redfield equation under driving.[3] The appropriate modifications to take into account excitation trapping and recombination are described in the main body of the manuscript. The corresponding steady-state Redfield equations in the eg and ee sectors read as

$$0 = -\mathrm{i}\left(\frac{\omega_x - \omega_c}{\gamma} - \mathrm{i}(\tau_c\gamma)^{-1} \right) \langle x|\rho_{eg}^{ss}|g\rangle + \frac{\mathrm{i}}{\hbar\gamma} I_0 \langle x|\mu_{eg}|g\rangle - \gamma^{-1} \sum_{x'} \left(\sum_{\tilde{x}} \mathrm{Re}\,\Gamma_{x\tilde{x}\tilde{x}x'} \right) \langle x'|\rho_{eg}^{ss}|g\rangle, \tag{S16}$$

$$\begin{aligned} 0 = {} & -\mathrm{i}\frac{\omega_x - \omega_{\bar{x}}}{\gamma} \langle x|\rho_{ee}^{ss}|\bar{x}\rangle + \frac{\mathrm{i}}{\hbar\gamma} \langle \bar{x}|\rho_{eg}^{ss}|g\rangle^* \langle x|\mu_{eg}|g\rangle - \frac{\mathrm{i}}{\hbar\gamma} \langle \bar{x}|\mu_{eg}|g\rangle^* \langle x|\rho_{eg}^{ss}|g\rangle \\ & + \gamma^{-1} \sum_{\bar{x}'x'} \left(\mathrm{Re}\,\Gamma_{\bar{x}'\bar{x}xx'} + \mathrm{Re}\,\Gamma^*_{x'x\bar{x}\bar{x}'} - \delta_{\bar{x}'\bar{x}} \sum_{\tilde{x}} \mathrm{Re}\,\Gamma_{x\tilde{x}\tilde{x}x'} - \delta_{x'x} \sum_{\tilde{x}} \mathrm{Re}\,\Gamma^*_{\bar{x}\tilde{x}\tilde{x}\bar{x}'} \right) \langle x'|\rho_{ee}^{ss}|\bar{x}'\rangle \\ & + \gamma^{-1} \left\langle x \left| \mathcal{L}_{\mathrm{rec}}[\rho_{ee}^{ss}] \right| \bar{x} \right\rangle + \gamma^{-1} \left\langle x \left| \mathcal{L}_{\mathrm{RC}}[\rho_{ee}^{ss}] \right| \bar{x} \right\rangle, \end{aligned} \tag{S17}$$

where the tetradic quantity $\Gamma_{\bar{x}x\bar{x}'x'}$ is

$$\Gamma_{\bar{x}x\bar{x}'x'} = \sum_j \langle \bar{x}|j\rangle\langle j|x\rangle\langle \bar{x}'|j\rangle\langle j|x'\rangle \int_0^{+\infty} \mathrm{d}s\, \frac{C(s)}{\hbar^2} \exp\left(\mathrm{i}(\omega_{x'} - \omega_{\bar{x}'})s\right). \tag{S18}$$

In Eqs. (S16) and (S17), we follow a common practice and neglect imaginary parts of $\Gamma_{\bar{x}x\bar{x}'x'}$. For the Drude–Lorentz spectral density, and under the assumption of purely real exciton wave functions $\langle j|x\rangle$, the corresponding real parts can be computed analytically to yield

$$\mathrm{Re}\,\Gamma_{\bar{x}x\bar{x}'x'} = \left[\sum_j \langle \bar{x}|j\rangle\langle j|x\rangle\langle \bar{x}'|j\rangle\langle j|x'\rangle \right] \mathcal{C}(\omega_{x'} - \omega_{\bar{x}'}), \tag{S19}$$

where

$$\mathcal{C}(\omega) = \mathrm{Re} \int_0^{+\infty} \mathrm{d}s\, C(s)\, \mathrm{e}^{\mathrm{i}\omega s} = \begin{cases} \frac{1}{2} \times \frac{2\pi}{\hbar} \times \left(\frac{2}{\pi} \lambda \frac{\omega\gamma}{\omega^2+\gamma^2} \right) (1 + n_{\mathrm{BE}}(\omega)), & \omega > 0; \\ \frac{1}{2} \times \frac{2\pi}{\hbar} \times \left(\frac{2}{\pi} \lambda \frac{|\omega|\gamma}{|\omega|^2+\gamma^2} \right) n_{\mathrm{BE}}(|\omega|), & \omega < 0; \\ 2 \times \frac{\lambda}{\hbar\gamma} \times \frac{k_B T}{\hbar}, & \omega = 0. \end{cases} \tag{S20}$$

Upon solving Eqs. (S16) and (S17), we explicitly check that the continuity equation $J_{\mathrm{gen}} - J_{\mathrm{rec}} - J_{\mathrm{RC}} = 0$ is satisfied.

The convergence of the HEOM method should always be checked against the maximal depth of the hierarchy and the number of terms in the optimized exponential series for the bath correlation function. Let us first concentrate on the convergence with respect to the depth of the hierarchy. We gradually increase the depth of the hierarchy in the following manner:

1. we start with Eqs. (S10) and (S11) up to depth $D = 2$; the initial guess for the RDM is obtained by solving Eqs. (S16) and (S17), while the ADMs on depths 1 and 2 are set to zero; the numerical accuracy with which the continuity equation is satisfied is set to δ_2, see Eq. (S12);

2. we use the solution up to depth $D \geq 2$ as the initial guess for the computations up to depth $D+2$ (the ADMs at depths $D+1$ and $D+2$ are set to zero); the numerical accuracy with which the continuity equation is satisfied in the computation up to depth $D+2$ is $\delta_{D+2} = c \cdot \delta_D$, where $c < 1$ (if the numerical accuracy is not downscaled, the algorithm at depth $D+2$ terminates immediately).

In this manner, we are able to check how the quantities of our interest, in particular transformation parameters between exciton/localized basis and the preferred basis of the NESS, depend on the maximal depth of the hierarchy. For the values of model parameters summarized in Table I of the main text, the deepest hierarchy is constructed for the largest reorganization energy ($\lambda = 400\,\mathrm{cm}^{-1}$), and its depth is 14.

We now briefly discuss the convergence of the HEOM with respect to K, and concentrate on the values of model parameters listed in Table I of the main text. These values satisfy the low-temperature approximation $\beta\hbar\gamma \ll 1$ reasonably well. When the interaction with the environment is weak, the steady-state Redfield equations [Eqs. (S16) and (S17)] should present a good description of the situation of our interest. From Eqs. (S18)–(S20), we see that, in this case, the relaxation tensor depends on the full spectral density, so that we should have $K > 1$. We have checked that $K = 3$ is a reasonable choice for the weak coupling to the environment. On the other hand, for stronger excitation–environment coupling, we have numerically verified that it is enough to take $K = 1$.

SIII. ANALYSIS OF THE DYNAMICS INITIATED BY A δ-LIKE PHOTOEXCITATION

Here, we analyze in greater detail the dynamics of the model dimer initiated by an impulsive photoexcitation and extract the time scales of such dynamics. In particular, we examine time dependence of the real and imaginary part of the interexciton coherence on a picosecond time scale following a sudden δ-like excitation at $t = 0$. The real part of the interexciton coherence is fitted using

$$\mathrm{Re}\left\{\rho_{01}(t)\right\} = a_0 + a_1\, e^{-t/a_2} \cos(a_3 t) + a_4\, e^{-t/a_5} + a_6\, e^{-t/a_7}, \tag{S21}$$

while the fitting function for the imaginary part reads as

$$\mathrm{Im}\left\{\rho_{01}(t)\right\} = b_1\, e^{-t/b_2} \sin(b_3 t) + b_4\, e^{-t/b_5} + b_6\, e^{-t/b_7}. \tag{S22}$$

In Fig. SI, we present the results of computations and fit, while the best values of fitting parameters are summarized in Tables SI–SIV.

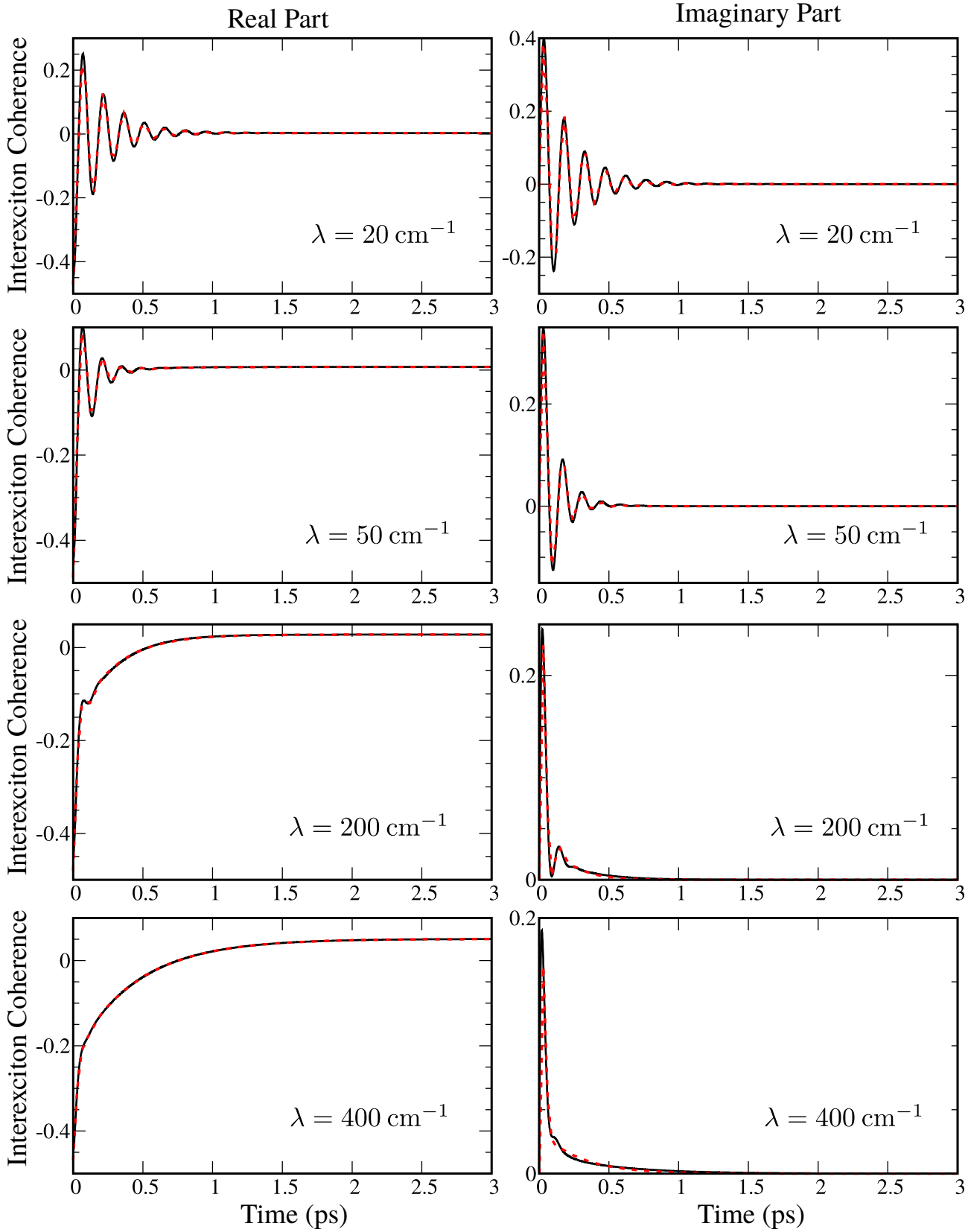

FIG. SI. Time dependence of the real (left column) and imaginary (right column) part of the interexciton coherence following a sudden δ-like excitation of the model dimer. Solid lines are obtained by propagating HEOM, while dashed lines are best fits to numerical data using the fitting functions given in Eqs. (S21) and (S22). The best fitting parameters are summarized in Tables SI–SIV.

TABLE SI. Fitting Parameters for $\lambda = 20\,\mathrm{cm}^{-1}$.

Parameter (Unit)	Value
a_0 (-)	2.96×10^{-3}
a_1 (-)	-0.3933
a_2 (fs)	193.9
$\hbar a_3$ (cm^{-1})	228.5
a_4 (-)	-0.091
a_5 (fs)	84
a_6 (-)	0.010
a_7 (fs)	300
b_1 (-)	0.4460
b_2 (fs)	192.8
$\hbar b_3$ (cm^{-1})	229.1
b_4 (-)	-0.0277
b_5 (fs)	103
b_6 (-)	0.0209
b_7 (fs)	282

TABLE SII. Fitting Parameters for $\lambda = 50\,\mathrm{cm}^{-1}$.

Parameter (Unit)	Value
a_0 (-)	7.24×10^{-3}
a_1 (-)	-0.3146
a_2 (fs)	105.2
$\hbar a_3$ (cm^{-1})	235.7
a_4 (-)	-0.03135
a_5 (fs)	277
a_6 (-)	-0.14762
a_7 (fs)	60.70
b_1 (-)	0.43085
b_2 (fs)	99.20
$\hbar b_3$ (cm^{-1})	240.6
b_4 (-)	-0.06465
b_5 (fs)	165.2
b_6 (-)	0.0526
b_7 (fs)	148.0

TABLE SIII. Fitting Parameters for $\lambda = 200\,\mathrm{cm}^{-1}$.

Parameter (Unit)	Value
a_0 (-)	0.02787
a_1 (-)	-0.163
a_2 (fs)	51.4
$\hbar a_3$ (cm^{-1})	230
a_4 (-)	-0.141
a_5 (fs)	43.9
a_6 (-)	-0.2038
a_7 (fs)	270.7
b_1 (-)	0.427
b_2 (fs)	36.9
$\hbar b_3$ (cm^{-1})	250
b_4 (-)	-0.0754
b_5 (fs)	15.92
b_6 (-)	0.0662
b_7 (fs)	156.7

TABLE SIV. Fitting Parameters for $\lambda = 400\,\mathrm{cm}^{-1}$.

Parameter (Unit)	Value
a_0 (-)	0.050754
a_1 (-)	-0.082
a_2 (fs)	42.80
$\hbar a_3$ (cm^{-1})	222
a_4 (-)	-0.163
a_5 (fs)	44.7
a_6 (-)	-0.2746
a_7 (fs)	446.5
b_1 (-)	0.8
b_2 (fs)	19.5
$\hbar b_3$ (cm^{-1})	170
b_4 (-)	-0.0496
b_5 (fs)	16
b_6 (-)	0.0349
b_7 (fs)	277

SIV. TRANSFORMATION PARAMETERS θ_{pl} AND Δ_{pl} UNDER FAST TRAPPING

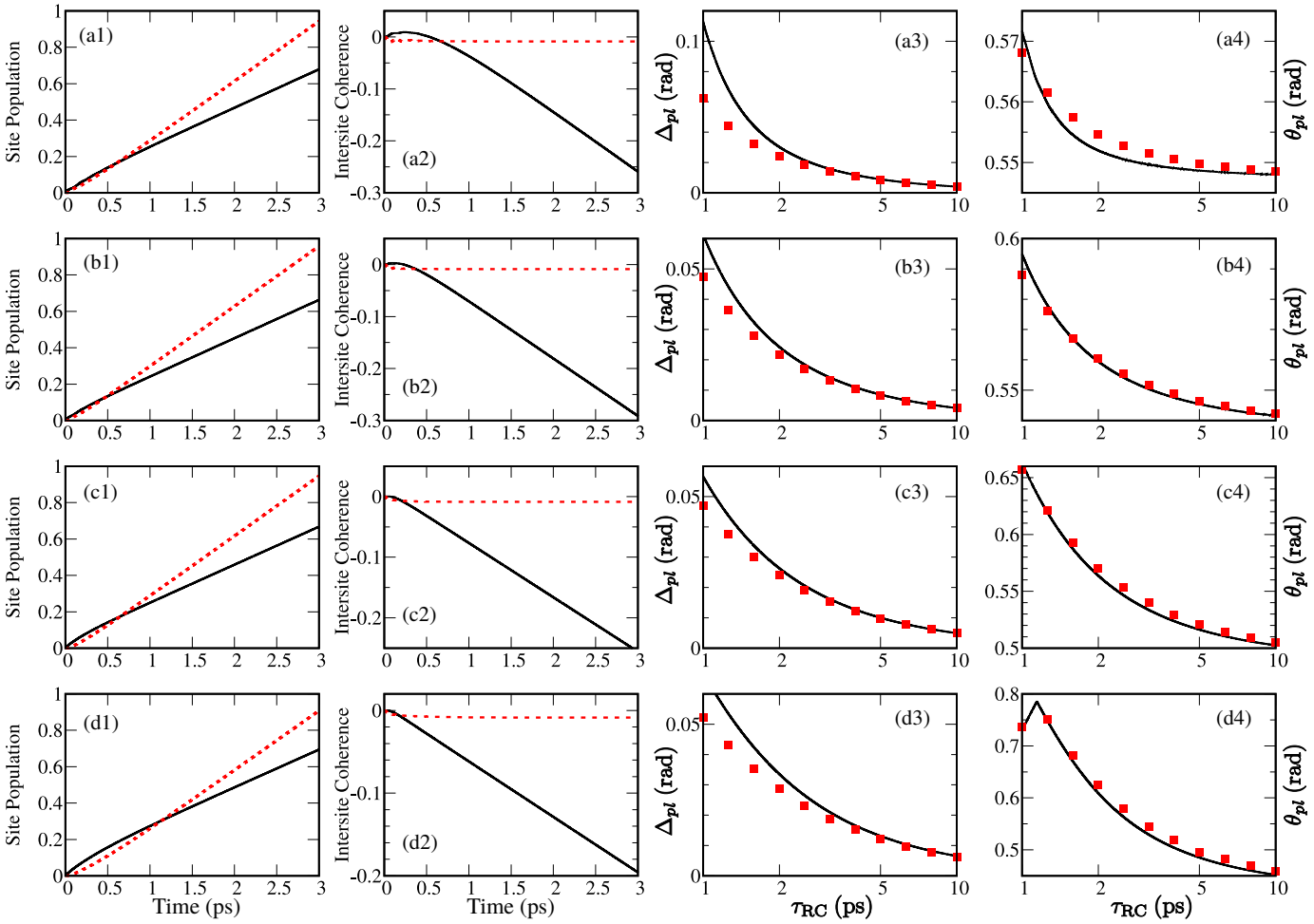

FIG. SII. (a1)–(d1): Time dependence of populations of localized states $|l_0\rangle$ (solid line) and $|l_1\rangle$ (dashed line) of the incoherently driven and unloaded model dimer for different values of the reorganization energy. (a2)–(d2): Time dependence of the real (solid line) and imaginary (dashed line) parts of the intersite coherence of the incoherently driven and unloaded model dimer for different values of the reorganization energy. Both site populations and intersite coherences are measured in units of $I_0\, d_{eg}^2/(\hbar\gamma)^2$. The excitation is suddenly turned on at $t = 0$. Dependence of the transformation parameters Δ_{px} [(a3)–(d3)] and θ_{px} [(a4)–(d4)] between the localized basis and the preferred basis of the NESS on the trapping time constant $\tau_{\rm RC} \in (1, 10)$ ps for different values of the reorganization energy. Solid lines are computed using time traces of a driven and unloaded model dimer at $t = \tau_{\rm RC}$, while squares emerge from the computation of the NESS using Eqs. (10) and (11) of the main text. The scale on the abscissa ($\tau_{\rm RC}$) in (a3)–(d4) is logarithmic. Trapping at the RC is governed by the localized-trapping Liouvillian [Eq. (18) of the main text]. The values of the reorganization energy are 20 $\rm cm^{-1}$ [(a1)–(a4)], 50 $\rm cm^{-1}$ [(b1)–(b4)], 200 $\rm cm^{-1}$ [(c1)–(c4)], and 400 $\rm cm^{-1}$ [(d1)–(d4)].

[1] H.-D. Zhang, Q. Qiao, R.-X. Xu, X. Zheng, and Y. Yan, "Efficient steady-state solver for hierarchical quantum master equations," J. Chem. Phys. **147**, 044105 (2017).
[2] Q. Shi, L. Chen, G. Nan, R.-X. Xu, and Y. Yan, "Efficient hierarchical Liouville space propagator to quantum dissipative dynamics," J. Chem. Phys. **130**, 084105 (2009).
[3] V. Janković and T. Mančal, "Exact description of excitonic dynamics in molecular aggregates weakly driven by light," (2020), arXiv:2001.07180 [physics.chem-ph].